Electrical, thermal, and elastic properties of the *MAX*-phase Ti_2SC

T. H. Scabarozi,[1] S. Amini,[1] P. Finkel,[1] O. D. Leaffer,[1] J. E. Spanier,[1] M. W. Barsoum,[1] M. Drulis,[2] H. Drulis,[2] W. M. Tambussi,[3] J. D. Hettinger,[3] and S. E. Lofland[3,a)]
[1]*Department of Materials Science and Engineering, Drexel University, Philadelphia, Pennsylvania 19104, USA*
[2]*Polish Academy of Sciences, Trzebiatowski Institute of Low Temperature and Structure Research, P.O. Box 1410, 50-950 Wroclaw 2, Poland*
[3]*Department of Physics and Astronomy, Rowan University, Glassboro, New Jersey 08028, USA*

(Received 2 January 2008; accepted 20 May 2008; published online 1 August 2008)

We report on the electronic, thermal, and elastic properties of the layered ternary, Ti_2SC. Resistivity, Hall effect, and magnetoresistance were measured as a function of temperature between 2 and 300 K and at fields up to 9 T. The Hall coefficient is negative and roughly temperature independent. The transport results were analyzed within a two-band framework, with electrons as the dominant charge carrier. The room-temperature thermal conductivity ($\approx$60 W/m K) is the highest of any *MAX* phase measured to date, with a substantial phonon contribution. The specific heat was measured from 2 to 300 K, yielding a Debye temperature of 765 K and in agreement with the Debye temperature of 745 K found from ultrasonic time-of-flight measurements. Young's, shear, and bulk moduli from the latter measurements were 290, 125, and 145 GPa, respectively. The calculated values of the lattice parameters (a=3.2051 Å and c=11.2636 Å), and Young's, shear, and bulk moduli (329, 138, and 179 GPa, respectively), based on the results of density functional theoretical simulations, compare favorably with measurements. © *2008 American Institute of Physics*. [DOI: 10.1063/1.2959738]

I. INTRODUCTION

Machinable ternary carbides and nitrides with the general formula, $M_{n+1}AX_n$ (where M is an early transition metal, A is an A-group element, and X is C or N) represent a class of solids with an unusual combinations of properties.[1–3] Two independent basal slip systems render them exceedingly damage tolerant, thermal shock resistant, and relatively tough.[3] Their most characteristic attribute, however, has to be the ease by which most materials within this family can be machined.

Studies on bulk materials have shown that most of the carbon-based *MAX* phases—especially the Ti-containing ones—are compensated conductors in that the concentrations of electrons and holes are nearly equal.[4–8] Their electron and hole mobilities are also quite comparable. Consistent with their compensated nature, many *MAX*-phase compounds exhibit a thermopower near zero over a wide range of temperatures.[5–8]

Original synthesis of Ti_2SC powder was achieved by Kudielka and Rhode,[9] followed by Nowotny.[10] Sulfur containing ternaries, as well as P and As, have a considerably shorter c-axis lattice parameter than those of all other *MAX* compounds. This results in the lowest c/a ratio of the M_2AX (211) compounds and is thus expected to exhibit different transport properties. For instance, Nb_2SC is a known superconductor, with a transition temperature of 3–5 K depending on C concentration.[11]

This paper examines the physical properties of Ti_2SC to gain insight into its elastic, electronic, thermal, and magnetic transport properties. To achieve this goal, we measured the electrical resistivity ρ, magnetoresistance coefficient α, Hall coefficient R_H, thermal conductivity κ, Seebeck coefficient, and heat capacity c_p, of fully dense Ti_2SC, and compared the measurements to results of density functional theoretical simulations.

II. EXPERIMENTAL AND ANALYSIS DETAILS

The sample fabrication details are described elsewhere.[12] In general, samples were hot pressed in a vacuum atmosphere hot press starting with—325 mesh Ti_2SC powder (3-ONE-2 LLC, Voorhees, NJ). The powder was wrapped in graphite foil, placed in a graphite die and heated up at 10 °C/min to 1500 °C and held at that temperature for 5 h. The chamber was pressurized at 500 °C to a maximum pressure of ~45 MPa that was maintained throughout the process.

Electrical and thermal transport measurements were carried out on samples with dimensions $1\times1\times10$ mm^3. R_H, ρ, and the magnetoresistance MR, were measured as a function of temperature in the 2–300 K range and in magnetic fields up to 9 T. Thermopower and thermal conductivity were measured between 2 and 400 K. All measurements were performed on a Quantum Design Physical Properties Measurement System with a four-probe technique. The details of the experimental procedures can be found elsewhere.[4,7,8]

Ultrasonic echo-pulse measurement of longitudinal v_l and shear v_s sound velocities were carried out at room temperature on polished $8\times8\times8$ mm^3 cubes cut from the same batch used for the transport and thermal measurements. For room temperature, Salol® was used as a bonding compound for the lithium niobate ultrasonic transducer tuned at its fundamental frequency of 15 MHz. Both sound velocity measurements were performed on a RAM 10000 from Ritec which has a resolution of 10 ppm time-of-flight resolution.

a)Electronic mail: lofland@rowan.edu.

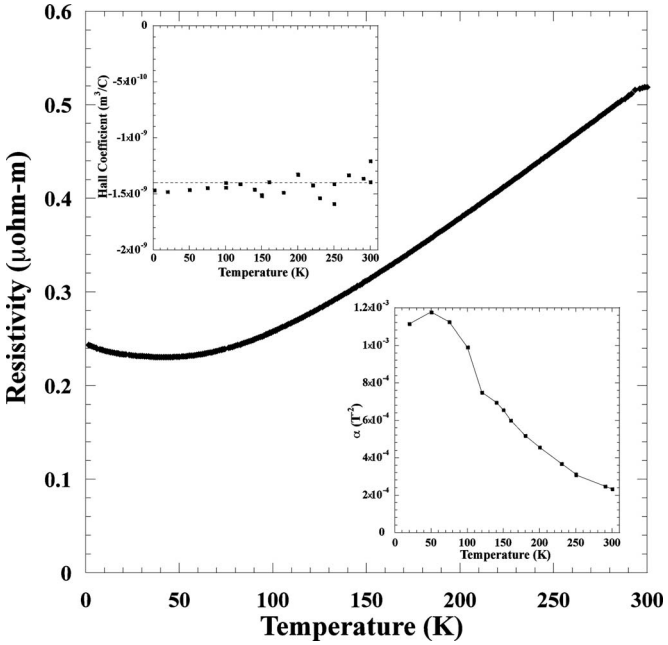

FIG. 1. Temperature dependence of resistivity. Note the linear temperature dependence at high temperatures and the slightly increasing value of resistivity at temperatures below 40 K. The upper-left inset shows the nearly temperature independent Hall coefficient, R_H. The dashed line in this inset is the average of R_H over that temperature range. The lower-right inset is the temperature dependence of the parabolic magnetic field dependence of the resistivity $\{\alpha B^2=\rho(B)-\rho(0)/[\rho(0)]\}$.

Other experimental details on this technique are discussed elsewhere.[8]

Raman spectra were taken at room temperature with a Renishaw 2000 spectrometer using Ar ion laser excitation (514.5 nm). Spectra were collected in static mode with ten accumulations with a 60 s exposure time. Experimental peak positions were calculated through Lorentzian fitting with a system resolution of 2 cm^{-1}.

Density functional theoretical (DFT) calculations of total energy, of interatomic forces, and of the stiffness tensor components were performed with the Vienna *ab initio* simulation package[13] (VASP) as implemented in MedeA (Materials Design, Angel Fire, NM), which has been used previously to predict energy-optimized structures in other *MAX* phases.[14] The relaxed lattice parameters and atomic positions were calculated by using the automated energy convergence in MedeA. Phonon and mechanical property calculations were started with the relaxed cell as the initial configuration. All calculations were done with a first-order Methfessel–Paxton smearing[15] with a width of 0.2 eV, and the generalized gradient approximation-Perdew, Burke and Ernzerhof/projector augmented-wave (GGA-PBE/PAW) (Refs. 16 and 17) pseudopotentials implemented by VASP (Ref. 18) using a 400 eV plane wave cutoff. These were chosen because of the metal-like electronic properties of the *MAX* phases. A $9\times9\times3$ k-point grid evenly spaced in the first Brillouin zone was used, chosen to be the same as the final k-point grid from the automated convergence, which was constrained to choose odd-sized grids. The moduli were calculated from the stiffness matrix which was calculated by perturbing the unit cell in five directions (necessitated by the hexagonal symmetry) to strains of 0.005, 0.01, and 0.02, calculating the energy after relaxing the atomic positions, and then using a least-squares fitting to determine the constants in the matrix.[19,20] The residual of the least-squares fitting was 3.7%.

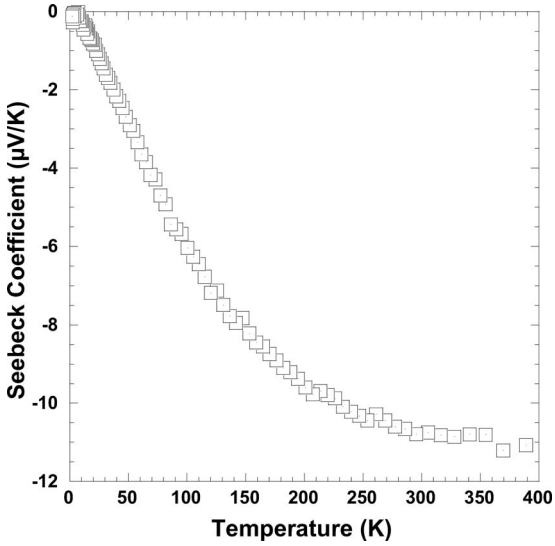

FIG. 2. Plot of the Seebeck coefficient as a function of temperature.

Phonon modes were calculated from MedeA's implementation of PHONON,[21] using the direct approach with two-point displacements where select atom positions were perturbed according to the symmetry of the cell giving partial derivatives for the energy. Modes were determined from the eigenvectors of the force matrix computed. The same optimized unit cell was used rather than a supercell because our interest was limited to the gamma point energies. Raman modes were identified based on their symmetry following Ref. 14.

III. RESULTS

Figure 1 displays the electrical resistivity as a function of temperature. The linearly decreasing temperature dependence of this material shows metallic-like conduction down

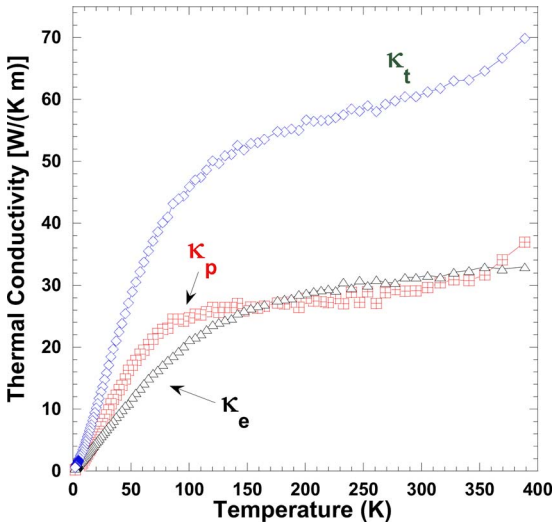

FIG. 3. (Color online) Temperature dependence of thermal conductivity. The solid squares represent the measured thermal conductivity, κ. Open triangles represent L_0T/ρ; solid triangles represent $k_p^{\min}$ determined by subtracting L_0T/ρ from κ.

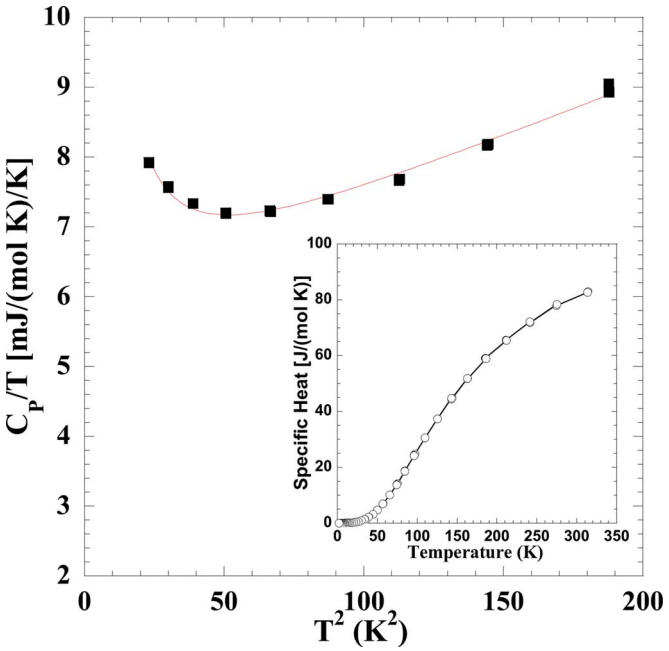

FIG. 4. (Color online) Plot of c_p/T vs T^2 at low temperatures. The increase at $T<7$ K is likely from a Schottky anomaly. The inset shows the c_p over the full temperature range measured.

to ~50 K. R_H, plotted as function of temperature, T, in the upper-left inset of Fig. 1, is relatively large, negative, and generally temperature independent. The lower-right inset of Fig. 1 is a plot of the temperature dependence of the MR coefficient, α, which is defined as $\{[\rho(B)-\rho(0)]/\rho(0) = \alpha B^2\}$, where $\rho(B)$ is the field-dependent resistivity. In general, the MR is positive, quadratic, and nonsaturating for all measured temperatures and magnetic fields up to 9 T.

The Seebeck coefficient as a function of temperature is shown in Fig. 2. At higher temperatures the thermopower is negative at roughly -10 μV/K. The thermal conductivity,κ, monotonically increases with temperature up to 390 K (Fig. 3). In Fig. 4, we present the low-temperature specific heat c_p/T as a function of T^2. The overall temperature dependence of c_p is shown as an inset.

Figure 5 shows the Raman spectra for Ti_2SC, which has four peaks associated with it. Table I lists experimental and

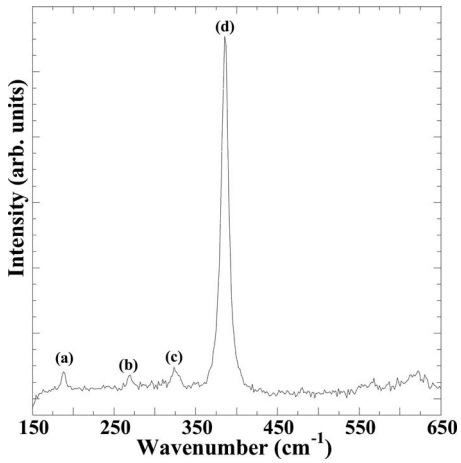

FIG. 5. Raman spectra at room temperature for Ti_2SC. Lorentzian fitted peaks are approximately (a) 188.1, (b) 269.9, (c) 325.4, and (d) 385.8 cm^{-1}.

TABLE I. Experimental and calculated Raman peak positions for Ti_2SC.

Measured positions (cm^{-1})	188	270	325	386
Calculated positions (cm^{-1})	185	264	315	381

calculated Raman peak positions, which are in excellent agreement. The longitudinal and shear sound velocities are $v_l \approx 8200$ m/s and $v_s \approx 5200$ m/s, respectively. Table II lists experimental and calculated physical properties such as the lattice constants and elastic moduli.

IV. DISCUSSION

A large negative Seebeck coefficient and relatively large and roughly temperature independent negative R_H indicates a single-band, n-type, conductor. In the low-field limit of the single-band model, the following apply:

$$\sigma = \frac{1}{\rho} = en\mu_n, \tag{1}$$

$$R_H = \frac{1}{en}, \tag{2}$$

$$\alpha = \mu_n^2, \tag{3}$$

where n is the electron carrier density, μ_n is the electron mobility, e is the charge of an electron, and σ the electrical conductivity. This simple set of expressions allows a check for consistency between the temperature dependence of ρ and the transport data that can be extracted through the application of a magnetic field. For example, the magnitude and temperature dependence of ρ can be estimated from R_H and α. However, when these values are used, we find a temperature dependent ρ that is a factor of five *smaller* than the measured ρ.

Thus in order to properly analyze this system, a two-band model, used on most *MAX* phases studied to date, is required. In the low-field limit of the two-band model, the following apply:

$$\sigma = \frac{1}{\rho} = e(n\mu_n + p\mu_p), \tag{4}$$

$$\alpha \frac{\mu_n\mu_p np(\mu_n+\mu_p)^2}{(\mu_n+\mu_p p)^2}, \tag{5}$$

TABLE II. Comparison of experimental and calculated properties of Ti_2SC.

Parameter	Experimental value	Calculated value
a (nm)	0.3204	0.3205
c (nm)	1.1211	1.1264
v_l (m/s)	8200	8836
v_s (m/s)	5200	5446
E (GPa)	290	329
B (GPa)	145	179
μ (GPa)	125	138
ν	0.16	0.19
Θ_D (K)	765 ± 15, 745	735

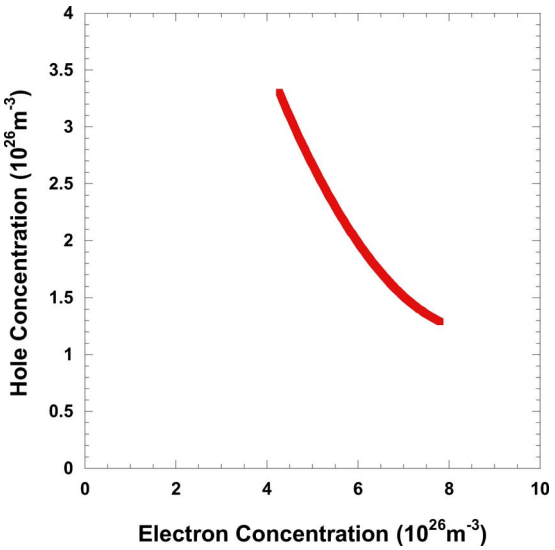

FIG. 6. (Color online) Allowed values for n and p, calculated from a two-band model.

$$R_H = \frac{(\mu_p^2 p - \mu_n^2 n)}{e(\mu_p p + \mu_n n)^2}, \tag{6}$$

where p is the hole carrier density; μ_p is the respective mobility. As there are four unknowns and three equations, a unique solution is not possible; however, it must be kept in mind that for all measurements at all fields and temperatures, there was no deviation from low-field behavior, implying that the scattering criterion of $\mu_n B$, $\mu_p B \ll 1$ is satisfied. Assuming $\mu B = 0.5$ and a maximum field of 10 T, this puts an upper limit on μ_n and μ_p of 0.05 $m^2/V\,s$. Note that the selected criterion is not very restrictive since deviations from the low-field model would be expected in this case. Since n and p are independent of temperature for metal-like conductors which has been confirmed for most *MAX* phases examined to date,[4,7,8] the low-temperature results, where the mobility is highest, yield the graph shown in Fig. 6 for the allowed n and p values. Since the Seebeck is negative, we anticipate that $n > p$; i.e., 4×10^{26} $m^{-3} < n < 8 \times 10^{26}$ m^{-3} and 1.5×10^{26} $m^{-3} < p < 3.5 \times 10^{26}$ m^{-3}. These values are about an order of magnitude smaller than those of other carbide *MAX* phases.[22]

The room-temperature value for κ (≈ 60 W/m K) is the largest measured in any *MAX*-phase material to date. Charge carriers and phonon transport entropy so, $\kappa = \kappa_e + \kappa_p$, where κ_e is the thermal conductivity due to the charge carriers and κ_p that due to the phonons. According the Wiedemann–Franz law

$$\frac{\kappa_e \rho}{T} = 2.45 \times 10^{-8} = L_0, \tag{7}$$

where L_0 is the Lorenz number. It is known that the value of L_0 is only correct at temperatures or much lower or higher than Debye temperature. Using L_0 at all temperatures provides an upper limit on the thermal conductivity due to charge motion and a minimum contribution from the phonon channel which will be designated as $\kappa_p^{\min}$. Application of this expression allows an extraction of $\kappa_p^{\min}$ from κ using the following:

$$\kappa = \kappa_p + \kappa_e = \kappa_p^{\min} + \frac{L_0 T}{\rho}. \tag{8}$$

After performing this manipulation of the data, we find that $L_0 T/\rho$ and $\kappa_p^{\min}$ are nearly equal over most of the temperature range measured (Fig. 3). This indicates that the enhanced thermal conductivity is a result of a large contribution from the phonon channel in comparison to that of other *MAX*-phase materials. A large phonon contribution to κ suggests a stiff material. This conclusion is consistent with the A-group element not rattling in the structure, as typical for all other A-group elements except Al, which is also relatively well bound.[2]

For most metal-like conductors, including the *MAX* phases, c_p is given as

$$c_p = \gamma T + \beta T^3 \tag{9}$$

at low temperature T, where γ is related to the electronic density of states, $N(E_F)$, and β relates to the phonon excitations. The data shown in Fig. 4 cannot be fit with Eq. (9) because of the increase in c_p at $T < 7$ K. This increase is most likely due to a Schottky anomaly. At temperatures where $k_B T >> \varepsilon$, where k_B is Boltzmann's constant and ε the energy difference between the two low-lying levels, c_p from a Schottky anomaly depends on temperature as AT^{-2}. Fitting the data with the sum of the three contributions yields a reasonably good fit with the fitting parameters γ, β, and A per unit cell being 11.2 mJ/mole K^2, 0.034 mJ/mole K^4, and 480 mJ/mole, respectively.

The γ term for Ti_2SC is in agreement with that found for other Ti-based 211 *MAX* phases and is given by

$$\gamma = \frac{(1+\lambda)\pi^2 k_B^2 N(E_F)}{3}, \tag{10}$$

where λ is the electron-phonon coupling. Setting $\lambda = 0.2$ (an approximate value for other Ti-based carbide *MAX* phases),[22] one finds $N(E_F) \sim 5.7$ eV^{-1}/unit cell.

For the phonon contribution to c_p, the characteristic parameter is the Debye temperature Θ_D, which is related to β by

$$\Theta_D^3 = \frac{12\pi^4 R x}{5\beta}, \tag{11}$$

where x is the number of atoms per formula unit and R is the gas constant. The values derived from the experimentally determined β are $\Theta_D = 765 \pm 15$ K. This is the largest value measured to date for a 211 material[23] and is commensurate with the values determined for the typically stiffer 312 *MAX*-phase materials and also consistent with the large phonon contribution to the thermal conductivity.

The Schottky-like anomaly probably arises from lattice defects. Such defects would be consistent with the upturn in the low-temperature resistivity and may be related with Fe impurities introduced during grinding of the powders since long collection time energy dispersive spectroscopy indicate about 2 wt % Fe. To test this, we synthesized Ti_2SC with 5 and 15 wt % Fe. Performing low-temperature c_p measurements and the analysis outlined above, we find a 10% and a 6% variation in γ and Θ_D, respectively, but a 400% increase

in the strength of the A term with increasing Fe content. This suggests that while the presence of Fe may produce lattice defects of an unknown type, which manifest in the presence of a Schottky anomaly, they have minimal impact on the intrinsic elastic and electronic properties; i.e., γ and Θ_D.

The elastic Debye temperature, Θ_s, is given by

$$\Theta_s = \frac{h}{k_B}\left[\frac{N v_l^3 v_s^3}{4\pi(v_s^3 + 2v_l^3)}\right]^{1/3}, \tag{12}$$

where h is Planck's constant and N is the number of atoms per unit volume. Using this expression, we find that Θ_s is 745 K, which is comparable to that determined from c_p.

The Poisson ratio

$$\nu = \frac{v_l^2 - 2v_s^2}{(2v_l^2 - 2v_s^2)} \tag{13}$$

of the $M_{n+1}AX_n$ phases generally lies between 0.19 and 0.22.[2] The present measurements yield ν=0.16, suggesting a weaker bonding anisotropy that of most *MAX* phases. The elastic moduli are defined by

$$E = v_s^2 \rho_M \frac{(3v_l^2 - 4v_s^2)}{(v_l^2 - v_s^2)},$$

$$\mu = \rho_M v_s^2,$$

$$B = \frac{\rho_M v_s^2}{3(1-2\nu)} \frac{3v_l^2 - 4v_s^2}{v_l^2 - v_s^2}, \tag{14}$$

where E, μ, and B are Young's, shear, and bulk moduli, respectively, and ρ_M the density of the material. Using these expressions, we find that E, μ, and B are 290, 125, and 145 GPa, respectively. In general, like other *ab initio* work on the *MAX* phases,[24–29] the agreement between theory and experiment is quite good. This coupled with the agreement between calculated and measured Raman spectra indicates a good understanding of the bonding in this material. We note in passing that while E and B are commensurate with those of most other 211 materials, the shear modulus is somewhat larger; approaching those in the 312 compounds.[2] We believe this, in part, explains the higher hardness of this material relative to the other *MAX* phases.[12]

This analysis suggests that Ti_2SC is unusual among *MAX*-phase family: the electronic carrier concentration is rather small, while elastic measurements indicate that this material is stiff, particularly in shear. This work relates to measurements on a material with A group from the VIA column of the Periodic Table which contains elements with high electron affinities. Enhanced bonding between S and the Ti-C units is consistent with all elastic and mechanical observations and with the observation that this material is not as readily machinable as other *MAX*-phase materials. We suspect that the origin of the increased modulus in this material is through a stronger bonding to the A-group planes, while in the 312 materials it is a result of a higher fraction of *M-X* bonds.

V. SUMMARY

The layered ternary, Ti_2SC, is an unusual *MAX* phase. The electrical conductivities, Hall coefficients, and magnetoresistances were analyzed within the low-field limit of a two-band framework, with electrons as the dominant charge carriers. Thermal transport results suggest that the phonon contribution to the thermal conductivity was as important as the electronic contribution. This suggests a stiff material, which agrees with ultrasonic time-of-flight measurements, yielding Young's, shear, and bulk moduli of 290, 125, and 145 GPa, respectively. Finally, the results of DFT simulations of lattice parameters, moduli, and zone-center phonon energies are in good agreement with experimental results.

ACKNOWLEDGMENTS

This work was supported by the NSF under Grant No. DMR 0503711. O.D.L gratefully acknowledges support from the U.S. Department of Education GAANN Fellowship under Award No. P200A060117.

[1] M. W. Barsoum, Prog. Solid State Chem. **28**, 201 (2000).
[2] M. W. Barsoum, in *Encyclopedia of Materials Science and Technology*, edited by R. W. C. K. H. J. Buschow, M. C. Flemings, E. J. Kramer, S. Mahajan, and P. Veyssiere (Elsevier, Amsterdam, 2006).
[3] M. W. Barsoum and M. Radovic, in *Encyclopedia of Materials Science and Technology*, edited by R. W. C. K. H. J. Buschow, M. C. Flemings, E. J. Kramer, S. Mahajan, and P. Veyssiere (Elsevier, Amsterdam, 2004).
[4] J. D. Hettinger, S. E. Lofland, P. Finkel, J. Palma, K. Harrell, S. Gupta, A. Gunguly, T. El-Raghy, and M. W. Barsoum, Phys. Rev. B **72**, 115120 (2005).
[5] H. I. Yoo, M. W. Barsoum, and T. El-Raghy, Nature (London) **407**, 581 (2000).
[6] M. W. Barsoum, H. I. Yoo, I. K. Polushina, V. Y. Rud, Y. V. Rud, and T. El-Raghy, Phys. Rev. B **62**, 10194 (2000).
[7] P. Finkel, B. Seaman, K. Harrell, J. D. Hettinger, S. E. Lofland, A. Ganguly, M. W. Barsoum, Z. Sun, S. Li, and R. Ahuja, Phys. Rev. B **70**, 085104 (2004).
[8] P. Finkel, M. W. Barsoum, J. D. Hettinger, S. E. Lofland, and H. I. Yoo, Phys. Rev. B **67**, 235108 (2003).
[9] H. Kudielka and H. Rhode, Z. Kristallogr. **114**, 447 (1960).
[10] H. Nowotny, Prog. Solid State Chem. **5**, 27 (1971).
[11] K. Sakamaki, W. Wada, H. Nozaki, Y. Onuki, and M. Kawai, Solid State Commun. **112**, 323 (1999).
[12] S. Amini, M. W. Barsoum, and T. El-Raghy, J. Am. Ceram. Soc. **90**, 3953 (2007).
[13] G. Kresse and J. Furthmuller, Phys. Rev. B **54**, 11169 (1996).
[14] J. E. Spanier, S. Gupta, S. Amer, and M. W. Barsoum, Phys. Rev. B **71**, 012103 (2005).
[15] M. Methfessel and A. T. Paxton, Phys. Rev. B **40**, 3616 (1989).
[16] J. P. Perdew, K. Burke, and M. Ernzerhof, Phys. Rev. Lett. **77**, 3865 (1996).
[17] P. E. Blöchl, Phys. Rev. B **50**, 17953 (1994).
[18] G. Kresse and J. Joubert, Phys. Rev. B **59**, 1758 (1999).
[19] Y. Le Page and P. Saxe, Phys. Rev. B **63**, 174103 (2001).
[20] Y. Le Page and P. Saxe, Phys. Rev. B **65**, 104104 (2002).
[21] K. Parlinski, Z. Q. Li, and Y. Kawazoe, Phys. Rev. Lett. **78**, 4063 (1997).
[22] S. E. Lofland, J. D. Hettinger, T. Meehan, A. Bryan, P. Finkel, S. Gupta, M. W. Barsoum, and G. Hug, Phys. Rev. B **74**, 174501 (2006).
[23] S. E. Lofland, J. D. Hettinger, K. Harrell, P. Finkel, S. Gupta, M. W. Barsoum, and G. Hug, Appl. Phys. Lett. **84**, 508 (2004).
[24] B. Holm, R. Ahuja, and B. Johansson, Appl. Phys. Lett. **79**, 1450 (2001).
[25] G. Hug and E. Frie, Phys. Rev. B **65**, 113104 (2002).
[26] G. Hug, M. Jaouen, and M. W. Barsoum, Phys. Rev. B **71**, 024105 (2005).
[27] N. Medvedeva, D. Novikov, A. Ivanovsky, M. Kuznetsov, and A. Freeman, Phys. Rev. B **58**, 16042 (1998).
[28] Z. Sun, S. Li, R. Ahuja, and J. M. Schneider, Solid State Commun. **129**, 589 (2004).
[29] Z. M. Sun and Y. C. Zhou, Phys. Rev. B **60**, 1441 (1999).